UPPSALA
UNIVERSITET

ELEKTRO-MFE 20012
Examensarbete 30 hp
Oktober 2020

Wave resource assessment using numerical wave modelling

Akash Vijay Kumar

Masterprogram i förnybar elgenerering
Master Programme in Renewable Electricity Production

UPPSALA
UNIVERSITET

Teknisk- naturvetenskaplig fakultet
UTH-enheten

Besöksadress:
Ångströmlaboratoriet
Lägerhyddsvägen 1
Hus 4, Plan 0

Postadress:
Box 536
751 21 Uppsala

Telefon:
018 – 471 30 03

Telefax:
018 – 471 30 00

Hemsida:
http://www.teknat.uu.se/student

Abstract

Wave resource assessment using numerical wave modelling

Akash Vijay Kumar

Wave resource assessment is the collection of site-specific meteorological data to estimate the wave potential in a region and is carried out to mitigate the risks involved in the setup of wave energy converters. Wave resource assessment has been typically done using wave buoys. But wave buoys are expensive and require constant maintenance for smooth operation. An alternative to wave buoys is numerical wave modelling. Numerical wave modelling uses mathematical models to generate computer simulations that describe wave parameters in a region.

This project is carried out in the region of Hvide Sande, a western port city of Denmark situated in the North Sea. Wave resource assessment is conducted for this region using the SWAN numerical wave model. The data from a wave buoy in the region is used to perform comparative analysis, in order to study the SWAN wave model and to compare the accuracy of the wave data between the measured buoy and the calculated model. The accuracy of the numerical predictions is further quantified by using a correlation coefficient and the relative square root error. This is followed by a scatter diagram for the region to find the most frequent sea states. The corresponding energy flux of the most frequent sea states was found to be in the range of 1-5 kW/m and the highest energy flux for the area is about 40 kW/m for the region.

Handledare: Tatiana Potapenko
Ämnesgranskare: Malin Göteman
Examinator: Irina Temiz
ELEKTRO-MFE 20012

Popular scientific summary

Ocean wave power is a promising form of renewable power. Unlike its renewable counterparts such as solar and wind power, ocean wave power is more predictable and is less prone to interruptions. These factors coupled with its large potential make ocean wave power a possible solution to the increasing global energy demand.

Wave energy converters are used to harness the ocean wave energy to produce electricity. But to maximise the total electricity produced and to ensure smooth operation of these wave energy converters, they need to be placed at optimum wave sites or areas where the ocean wave potential is high. These sites are located through wave resource assessment. Wave resource assessment involves the collection of site-specific wave data to estimate the wave potential in a region. This is done to mitigate risks and maximise production when setting up of wave energy converters or wave farms. Hence, wave resource assessment is an important step when designing and deploying wave energy converters. Wave resource assessment is typically done by deploying wave buoys at regions of interest and analysing the wave data captured by the buoy. But the economic cost and time required of designing, deploying, and maintaining these wave buoys is high. An alternative method for wave resource assessment is through numerical wave models.

Numerical wave models use mathematical models to generate computer simulations that describe wave parameters. These wave parameters can then be used to assess the wave potential in the region. This thesis focuses on the use of a numerical wave model to perform wave resource assessment in the region of Hvide Sande, Denmark. The thesis covers the design and detailed study of the numerical wave model. Wave resource assessment is then carried out through the numerical wave model for the region of Hvide Sande. The accuracy of the results calculated by the wave model are compared to wave data from a wave buoy deployed in the same region. Based on the comparative results we can conclude the accuracy of the numerical wave model and its overall effectiveness in regard to time and cost. The thesis also covers a numerical analysis between the, model calculated wave data and the buoy measured wave data. The thesis concludes with graphical scatter plots that show the most frequent sea states of the region, through which the wave potential can be calculated.

Acknowledgment

Throughout the writing of this master thesis, I have received a great deal of support and assistance.

I would first like to thank my supervisor, Tatiana Potapenko whose continued guidance, and expertise was invaluable in formulating the methodology and research involved in the thesis. Your feedback encouraged me to improve my work and brought my thesis to a higher level.

I would like to acknowledge my subject reader Malin Göteman for her support, and my program director Irina Temiz for the opportunity to work in the field of wave power. I would also like to thank my program coordinator Juan de Santiago for his continued assistance and patience throughout my master studies.

I would like to thank my parents and brother, without whom I would not have the opportunities I do right now, and for their continued support throughout my journey. I could not have completed my master studies without the support of my friends, who provided well needed distractions to relax my mind outside of my work.

Lastly, I would like to thank all my colleagues and friends who I have met throughout this incredible journey. My interactions with each and every single one of you, have shaped my views and helped me better myself. Tack!

List of figures

Contents

1 Introduction

1.1 Background

The worldwide consumption of energy has rapidly increased over the last few years with a large portion of the energy being produced through fossil fuels. The continued reliance on non-renewable forms of energy with its already depleting resources is unrealistic and with increasing environmental damage associated by the use of fossil fuels, it is clear that alternative sources of energy are required to sustain our energy needs.

This is where renewable sources of energy play a major role. Energy obtained through natural sources and with its inexhaustible or constantly replenishing ability and its clear environmental benefits over its fossil fuel counterparts, renewable energy seems to be the key to a clean energy future. This has led to a rise in renewable power generation over the last decades as indicated in Fig. 1.

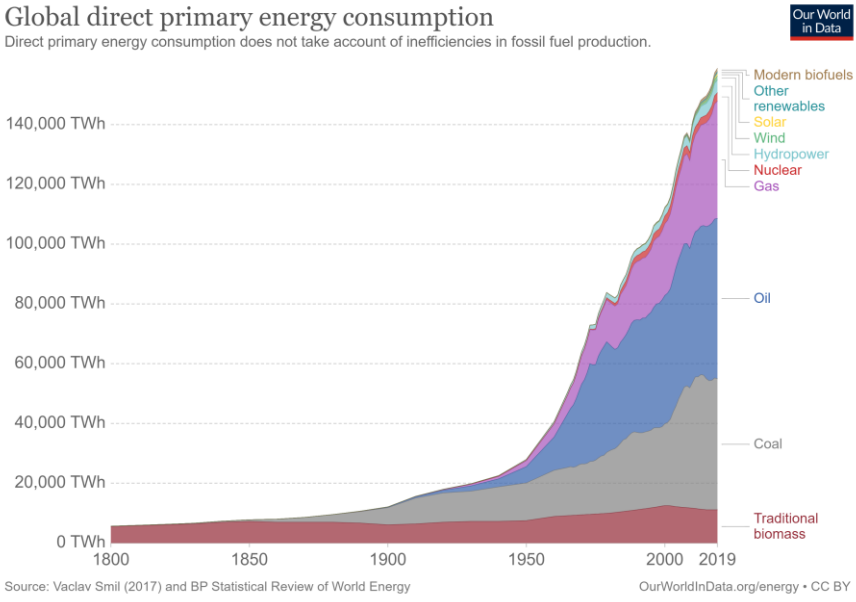

Figure 1.1. World energy consumption over the last decades [1]

But a major barrier to most forms of renewable energy include its unpredictability or variability of the renewable energy source. Wave power with its large potential offers a solution to the impending energy crisis and could greatly benefit society.

Ocean wave energy is a compounded and concentrated form of energy with an estimated global power potential of over 4000 TWh/ year [2].

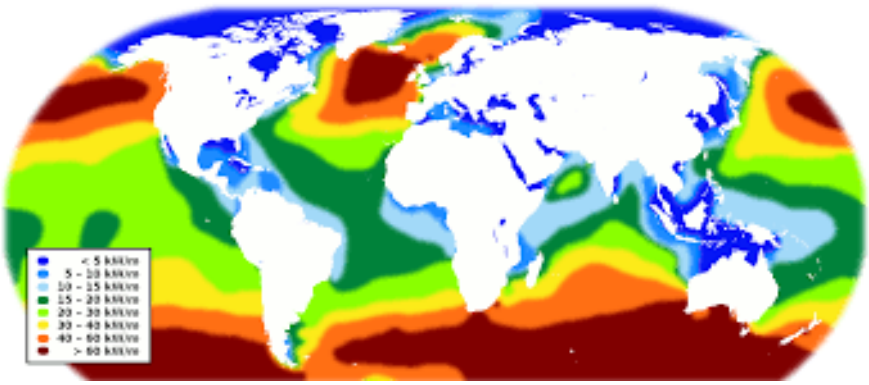

Figure 1.2. Global wave power potential

Ocean surface waves are formed due to the movement of wind over the ocean surface. Ripples along the surface of the ocean allow for wind to transfer energy onto the ocean surface generating wind waves. As winds continue to blow along the ocean's surface, larger and larger waves are created. The length along the ocean's surface over which the winds blow unobstructed is known as fetch. So, high winds and a long fetch distance lead to stronger waves. The energy in these waves can then be harnessed by wave energy converters and transformed into electricity to generate wave power. Apart from its renewable nature, availability and high potential, wave power is considered as a reliable form of energy due to its low interruption of ocean waves and the ability to predict sea states in advance.

1.2 Wave resource assessment

Wave resource assessment is the collection of site-specific wave data to estimate the wave potential in the region. Wave resource assessment helps mitigate risk and uncertainty involved in setting up of wave energy converters by providing a detailed summary of the directional wave spectra over a period [3]. The wave power assessment process can be split into two distinct stages [4]:

1. The first stage involves the selection of a site in the region of interest. In this stage a comparative analysis is done considering factors such as proximity to land, electric grid availability, ocean wave conditions and others that influence site selection.
2. The second stage involves a quantitative analysis by which the wave resource at the site is analyzed.

The wave resource primarily includes the wave height and wave period in the region. These wave parameters can be used to estimate the potential wave energy in the region. Further, the more comprehensive and quantitative knowledge of the wave climate in a region, the easier it is for developers to optimize technology [5]. Wave resource assessment is usually done through the deployment of wave buoys or the use of numerical wave modeling.

1.2.1 Wave buoys

Wave buoys are devices that monitor ocean and weather data within oceans. Wave buoys utilize a range of sensors and equipment onboard to measure ocean wave data. Wave parameters such as wave height, wave period, wave direction is measured and transmitted to data sites either using high frequency signals or satellite communication. Further, buoys can also be used to detect chemical spills and act as emergency response. Buoys then are far superior to other physical wave monitoring devices in terms of data gathering and accuracy, but wave buoys come with large downsides. The cost of building and deployment of buoys are estimated at $170,000/buoy [6]. This cost is excluding repair which is estimated at a further $25,000/year. Further, ocean conditions overtime degrade the buoy and reduce the accuracy of its measurements requiring upkeep which adds additional costs while also being hazardous to personnel involved in the upkeep process. Wave buoys are also hindered by extreme weather conditions as well as human intervention involving collision damage to the buoy.

1.2.2 Numerical wave modelling

Wave models utilize mathematical models to generate computer simulations that describe physical conditions such as wave generation, propagation, and dissipation. The models can be utilized to assess wave parameters on a global scale.

With the development of numerical technologies and advent of improved computing platforms, wave assessment through numerical models are found to be cost effective, reliable and time saving [7]. Wave modelling is used in research and marine operations where operational wave forecasting, and production of data sets allows for long term wave statistics or hindcasting to be

performed. These results help in wave resource assessment [8]. Wave modelling and their roles can be broadly categorized into two as:

- To derive wave statistics for long term time series of ocean wave data. Here, meteorological data of the region is turned into long term wave data through wave models.
- To derive wave statistics at coastal areas for assessment of prospective wave energy converter sites. These sites need to account for specific areas and breaking of waves at the shore.

This project utilizes a numerical wave model to perform wave resource assessment in a region. The Simulating WAves Nearshore (SWAN) model is a type of numerical wave model that is being used here. SWAN which is developed at Delft University of Technology is a third-generation open source wave model that computes random wind generated waves in coastal regions [9].

1.3 UU-WEC Technology

The Uppsala University Wave Energy Converter (UU-WEC) is a point absorber-based wave energy converter (WEC). It consists of a heaving buoy connected to a submerged linear generator. The linear generator is a permanent magnet linear generator which is placed on the seabed [10].

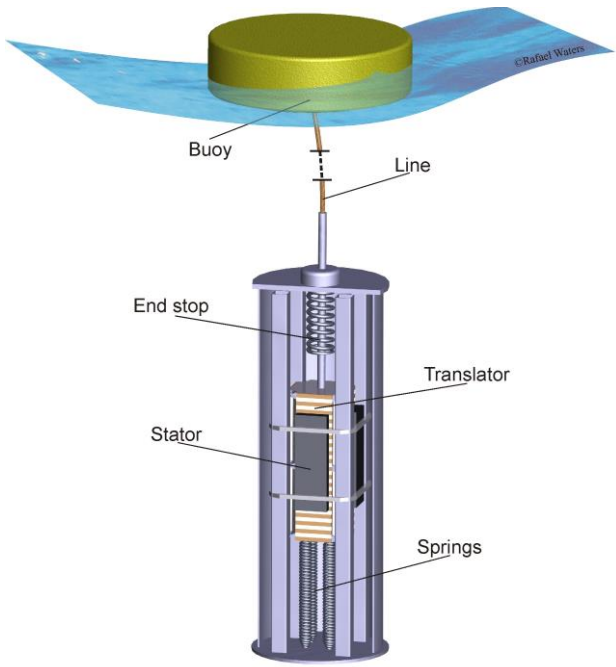

Figure 1.3. Uppsala University Wave energy converter [11]

The heaving buoy acts as the absorber and directly translates the movement of ocean waves into electrical power in bursts of varying frequency and amplitude. The presence of a linear generator negates the use of any intermediate steps in the conversion system. The UU-WEC has gone through many iterations including changes to the mechanical structure and the piston to improve its effectiveness in absorbing wave power as well as to improve survivability. Multiple UU-WEC's have been operational at the Lysekil wave energy research site and these WEC's are connected to an undersea substation before being transmitted onshore [12].

1.4 Studied region

The study is focused on the North Sea at the region of Hvide Sande, Denmark. Hvide Sande located at 56°N and 8.1°E is a port city on the western coast of Denmark lying on the edge of the North Sea.

The wave potential of the North Sea off the coast of Hvide Sande is comparatively lower than other regions but the lower sea states improve survivability of wave energy converters making this area suitable for the development of wave power. Hence, numerical wave modeling is used to estimate the wave potential in the region.

Additionally, a wave buoy has been deployed in the region. The wave buoy is located at 55°50'31.80" North latitude and 7°59'52.20 East longitude, just off the south-western coast of Hvide Sande. The deployed wave buoy is a Directional Waverider Mark II. The small spherical shaped buoy has a 0.9 m diameter and measures wave parameters and sea surface conditions. The buoy uses single point mooring and measures vertical acceleration by means of an accelerometer placed on a gravity stabilized platform which is suspended in a fluid with a plastic sphere placed at the bottom of the buoy [13].

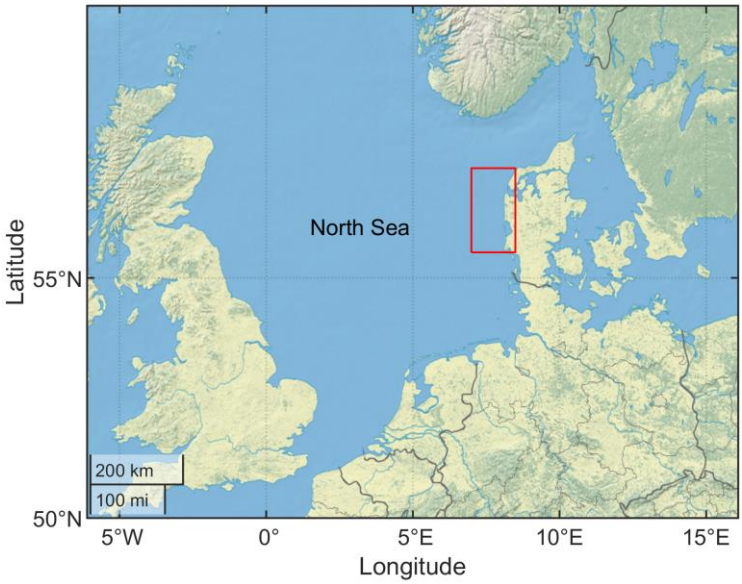

Figure 1.4. Region of interest located in the North Sea off the coast of Hvide Sande

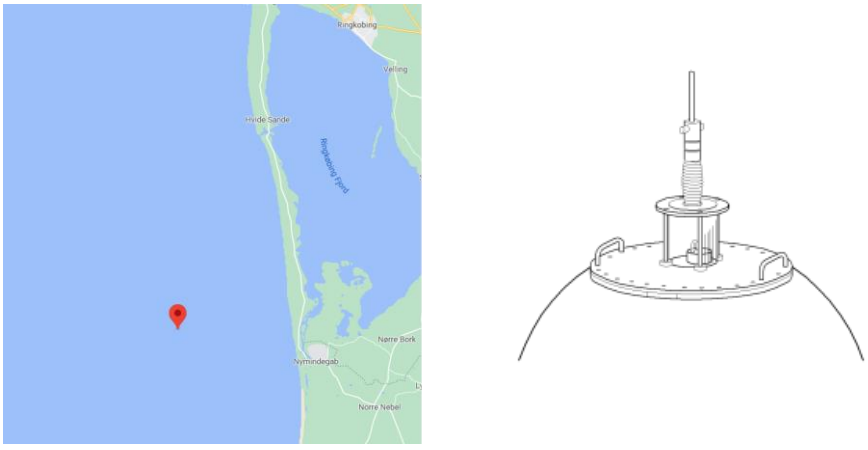

Figure 1.5. (left) Wave buoy location off the coast of Hvide Sande
(right) Representation of wave buoy Directional Waverider [13]

2 Theory

2.1 SWAN

SWAN is a third-generation advanced wind-wave model that solves the spectral action balance equation for the evolution of wave growth without any restrictions on the spectrum. SWAN accounts for deep water processes such as dissipation and wave propagation while also incorporating shallow water processes such as depth induced breaking, bottom friction and wave interactions.

The information contained within sea states which relate to wave parameters and wave propagation can be given by the energy density $E(\sigma, \theta)$ where σ the frequency of distribution of wave energy and θ is the direction of propagation. The energy density of sea states can be related by the action density which is given by $N = E/\sigma$. The action density unlike the energy density is conserved during wave propagation in the presence of ambient current which allows numerical wave models such as SWAN to calculate the evolution of action density given by $N(\vec{x}, t, \sigma, \theta)$ in space $\vec{x}$ and time t. This evolution of action density allows numerical wave models to determine wave propagation. The evolution or rate of change of action density is governed by the spectral action balance equation given by [14]:

$$\frac{\partial N}{\partial t} + \nabla_{\vec{x}} \cdot [(\overrightarrow{c_g} + \vec{U})N] + \frac{\partial c_\sigma N}{\partial \sigma} + \frac{\partial c_\theta N}{\partial \theta} = \frac{S_{tot}}{\sigma} \tag{2.1}$$

where $\frac{\partial N}{\partial t}$ denotes the kinetic portion of the action balance equation; $\nabla_{\vec{x}} \cdot [(\overrightarrow{c_g} + \vec{U})N]$ represents the propagation in 2D geographical space and $\overrightarrow{c_g}$ represents the group velocity including wave shoaling with N as the action density and $\vec{U}$ denotes ambient current; $\frac{\partial c_\sigma N}{\partial \sigma}$ represents the effect of shifting of radian frequency and $\frac{\partial c_\theta N}{\partial \theta}$ represents the refraction caused by depth and currents; σ relates to the frequency and θ is the propagation direction; S_{tot} represents the total physical processes of the wave spectra.

SWAN computes in a full spectrum thereby covering all directions and frequencies [15]. The total physical processes of the wave spectra can be split into six processes:

$$S_{tot} = S_{in} + S_{nl3} + S_{nl4} + S_{ds,w} + S_{ds,b} + S_{ds,br} \quad (2.2)$$

S_{in}: Wave growth by wind
S_{nl3} & S_{nl4}: Nonlinear transfer of wave energy through wave interaction
$S_{ds,w}, S_{ds,b}$ & $S_{ds,br}$: Wave decay due to whitecapping, bottom friction and depth induced wave breaking

These processes along with energy propagation in waves are being used in the computational process of SWAN. The different processes accounted for, in the SWAN computation are further discussed.

2.1.1 Wind waves

The irregular nature of wind causes irregular wave heights and wave periods to ocean waves. This leads to constantly varying ocean waves. Growth rates, swell propagation, turning winds and interaction between swell and wind are factors considered by the wave model. The SWAN model accounts for wind speed at a 10 m elevation and wave growth by wind is given by [16]:

$$S_{in}(\sigma, \theta) = A + BE(\sigma, \theta) \quad (2.3)$$

where, $S_{in}$is the wave growth by wind; BE describes the exponential growth with A describing the linear growth of wind; σ is the frequency and θ is the propagation direction.

The linear growth of wind, A is given by:

$$A = \frac{1.5 * 10^{-3}}{2\pi g^2}(U_* max[0, cos(\theta - \theta_w)])^4 H \quad (2.4)$$

where g is the acceleration due to gravity; $U_* max$ is the maximum friction velocity and θ_w is the wind direction; H is the filter that eliminates low frequencies. Computations using third generation wind-wave models without a low frequency filter causes misinterpretations with the physics of the model which leads to numerical errors [17]. Low wind speed errors and wind-sea interaction errors can be controlled by the use of a low frequency filter given by:

$$H = exp\{-(\frac{\sigma}{\sigma_{PM}^*})^{-4}\} \quad (2.5)$$

where σ_{PM}^* is the peak frequency of the fully developed sea state. The peak frequency acts as a range that helps improve numerical accuracy of the model by controlling lower frequency spectrum. The frequency is given by:

$$\sigma_{PM}^{*} = \frac{0.13g}{28U_{*}} 2\pi \tag{2.6}$$

The other aspect of wind growth is given by the exponential growth by wind given by:

$$B = max[0,0.25\frac{\rho_a}{\rho_w}(28\frac{U_{*}}{c_{ph}}cos(\theta - \theta_w) - 1]\sigma \tag{2.7}$$

In which c_{ph} is the phase speed and ρ_w, ρ_a are the densities of water and air.

These expressions form the basis upon which the wave model SWAN determines wind growth and wind-sea interaction.

2.1.2 Dissipation of wave energy

Dissipation of wave energy is dependent on three contributions: whitecapping, bottom friction and depth induced breaking.

2.1.2.1 Whitecapping

The measure of the steepness of the waves affects whitecapping. Whitecapping in the SWAN model uses a reformatted pulse-based model to be used in finite water depth [18]. The expression is given by:

$$S_{ds,w}(\sigma,\theta) = -\Gamma\bar{\sigma}\frac{k}{\bar{k}}E(\sigma,\theta) \tag{2.8}$$

where $\bar{\sigma}$ denotes the mean frequency and $\bar{k}$ denotes the mean wave number; Γ is the steepness coefficient and is dependent on the wind formulation used in the computation.

2.1.2.2 Bottom friction

Surface waves induce an orbital motion of water particles that propagate downwards. In shallow water, the orbital motion extends to the sea bed resulting in interactions between surface waves and the bottom. This causes distribution of wave energy and scattering of wave parameters. The distribution of wave energy and resultant scattering can be expressed by the bottom friction. SWAN uses the JONSWAP empirical model [19], the Eddy-viscosity model [20] and the drag law model for a bottom friction model. It is expressed as:

$$S_{ds,b} = -C_b\frac{\sigma^2}{g^2 sinh^2 kd}E(\sigma,\theta) \tag{2.9}$$

where C_b is the bottom friction coefficient and d is the depth.

2.1.2.3 Depth induced wave breaking

As waves propagate towards the shore, shoaling or the effect of decreasing wave depth increases the wave height. When the ratio of wave height over water depth increases beyond a certain limit, wave breaking takes place. The wave breaking causes energy dissipation. In shallower waters the effect of wave breaking increases. SWAN uses the bore-based model [21] to simulate energy dissipation of waves due to depth breaking. This is expressed as:

$$S_{ds,br}(\sigma,\theta) = \frac{D_{tot}}{E_{tot}} E(\sigma,\theta) \tag{2.10}$$

where E_{tot} is the total wave energy and D_{tot} is the dissipation of wave energy.

These processes impact the wave energy dissipation and are utilized by the numerical wave model to compute wave propagation.

2.2 Wave energy generation

Wave energy converters are responsible for the generation of electricity through ocean waves. Wave energy devices can broadly be classified based on their location:

- Offshore
- Nearshore
- Onshore

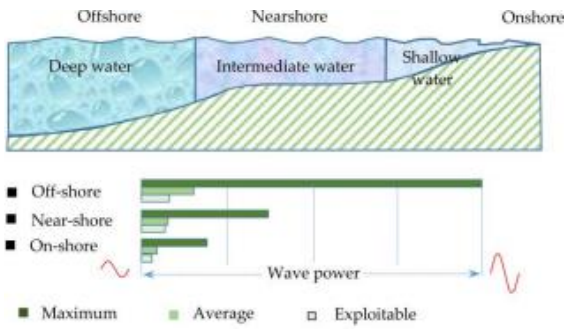

Figure 2.1. Wave energy converters based on position in the sea [22]

Onshore which relates to shoreline regions, where the water depth is 10-15 m. Nearshore regions have a water depth of 15-25 m. Offshore regions are based in deep water and have a water depth of over 50 m [22]. Wave power tends to

lose power density as it approaches the shoreline, so most wave energy devices are placed at offshore areas [22]. Further, near-shore and on-shore locations are battered by wave breaking requiring wave energy devices to be highly survivable [22].

WEC's are also classified based on the type of technology or the power take off system used, and they can be broadly categorized into:

1. Point absorber
2. Surface attenuator
3. Oscillating wave surge converter
4. Oscillating water column
5. Overtopping device
6. Submerged pressure differential
7. Floating in-air converters

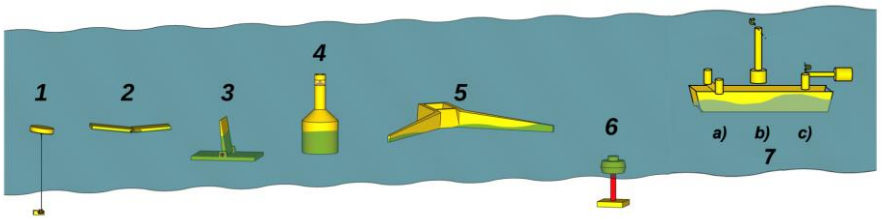

Figure 2.2. Different categories of WEC based on power take off systems used [23]

2.2.1 WEC stages

The stages involved in WEC's can be categorized as:

1. Absorption stage
2. Conversion stage
3. Generation stage

2.2.1.1 Absorption stage

In the first stage, WEC absorbs and converts the motion of waves into oscillating motion. The absorber in a WEC varies based on the type of WEC. The oscillating converter uses a flap, while the heaving point absorber based WEC uses a float as the absorber. Based on the absorber, different forces can be incident on the WEC [24]. The governing equation of WEC specified by Newton's II law is given by:

$$M\ddot{x} = F_{hyd} + F_{PTO} + F_{others} \tag{2.11}$$

In which $F_{hyd}, F_{PTO}, F_{others}$ are vectors describing hydrodynamic force, force by the power take off system and other forces incident on the absorber. The hydrodynamic force F_{hyd} can be broken down into the hydrostatic, wave excitation and radiation forces. These forces along with nonlinear forces and losses affect the absorption of a WEC.

2.2.1.2 Conversion stage

In this stage the absorbed energy is converted to useful energy. Because of irregular waves in the ocean there are extreme variations in power peaks and average power flow, hence it is necessary to reliably and efficiently convert the power absorbed by the waves. Depending on the type of absorber used, the method of conversion can involve pneumatic, hydraulic methods [24]. In some cases, like the UU-WEC, due to the use of linear generators the intermediate steps in the conversion stage can be excluded.

2.2.1.3 Generation stage

The generation stage involves the generation of electricity. The two types of generators to be considered include: linear generators and rotary generators. Linear generators do not require a conversion mechanism and is directly connected to the absorber while the rotary generator uses a conversion mechanism to be able to produce electricity.

Rotary generators are either fixed speed or variable speed generators while linear generators include permanent linear magnet generators or snapper. Each of the generators have varying advantages and disadvantages. The type of generator to be used depends on the losses, physical restrictions, and control strategies in place [24].

At this stage, electric power is generated through the WEC, now the generated electric power needs to be transmitted and connected to the electric grid.

2.2.2 Transmission systems for wave power

The transmission stage also consists of the conditioning stage where the generated electric power is connected to the electric grid. In order to connect to the main electric grid and to ensure stability within the grid, it is imperative that the frequency of the generated power matches with the frequency of the grid, especially in the case of varying speed generators.

The transmission stage consists of connecting the WEC or a wave power array to a substation interacting with transformers, converters, and cables before being connected to the grid.

2.2.2.1 Substation

Wave energy converters are connected to an underwater substation (UWS) either through a three-phase cable or two DC cables. In the case of using three-

phase cables, assuming multiple WEC's the control components are placed in the housing of the substation and includes transformers for converting power before transmission to shore. In the case of using DC cables, the control equipment is housed within the WEC.

There are various connection possibilities when connecting the WEC to the grid relating to position of the substation and converters. The positioning affects losses, cost, and material. Hence, based on the area of interest and the type of WEC employed a suitable connection system needs to be used. The various connection system possibilities are shown below [25]:

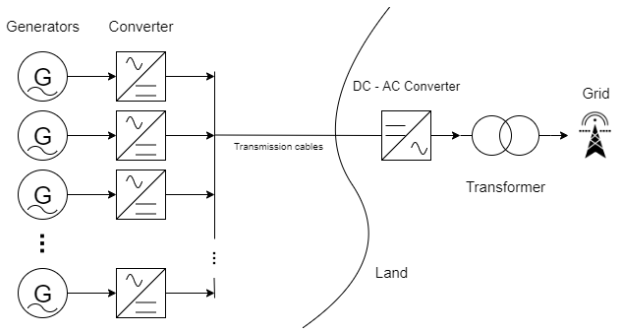

Figure 2.3. Connection possibility 1 – onshore converter [25]

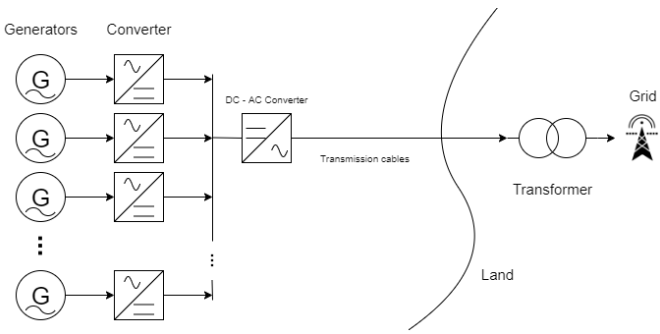

Figure 2.4. Connection possibility 2 – undersea converter [25]

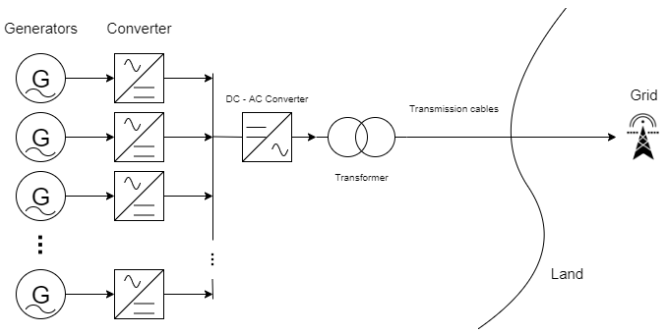

Figure 2.5. Connection possibility 3 – offshore converter and transformer [25]

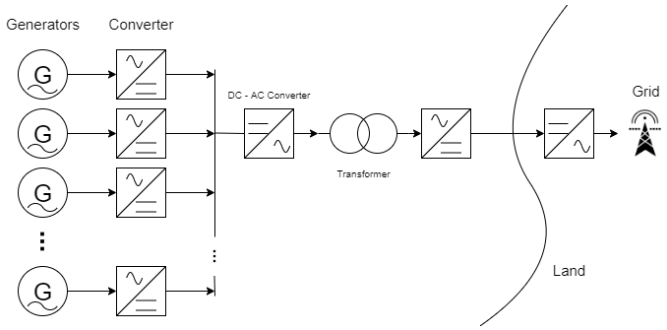

Figure 2.6. Connection possibility 4 – multiple converters with offshore transformer [25]

In connection 1, a series of WEC's are connected from the DC side. This is then transmitted through undersea transmission cables to a converter on land. The converter in connection with a transformer is used to connect to the grid. In this case the transformer used is a tap changer which mitigates voltage variations. In connection 2, The WEC's are connected to an undersea converter which is then connected to land. This connection increases complexity. Maintenance and survivability of undersea components needs to be considered here. In connection 3, both the converter and transformer are offshore. This allows for lower I^2R losses during transmission to land. The presence of undersea components increases complexity, but losses are reduced. In connection 4, the use of another converter after the transformer stage allows for high voltage DC (HVDC) transmission. This must then be converted back to AC before connecting to the grid. This connection possibility is highly complex due to the presence of multiple undersea components but provides better output due to reduced losses [25]. Based on the complexity and cable losses of the substation connection types, the following comparison can be inferred:

Table 1. *Comparison of connection type against complexity and cable losses*

Connection	Complexity	Cable loss
Connection 1	Low	High
Connection 2	Medium	Very high
Connection 3	High	Medium
Connection 4	Very high	Low

2.2.2.2 Shore transmission cable

Undersea cables are used in the transmission process to connect the WEC's to the shore/grid. On generation of electricity, DC cables carry the power to the shore or to other connection points such as substations. The WEC's can be connected to shore through different cabling connections. Cabling connection takes into account cost as well as reliability, hence prior to setting up of

WEC's a cabling connection analysis needs to be done in order to ascertain the best connection possibility for the chosen type of WEC and the area of interest [25]. The different cabling connections are discussed below,

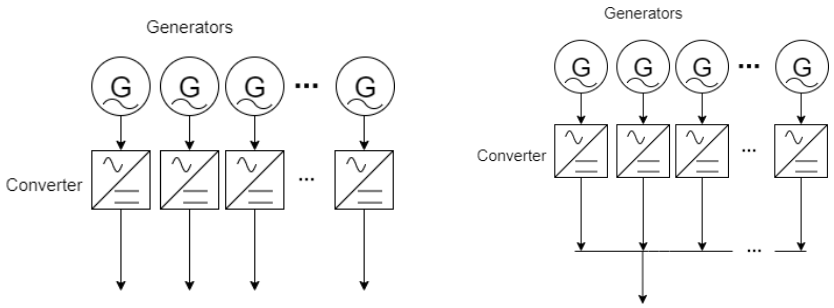

Figure 2.7. (left) Cabling connection type 1 and (right) cabling connection type 2 [25]

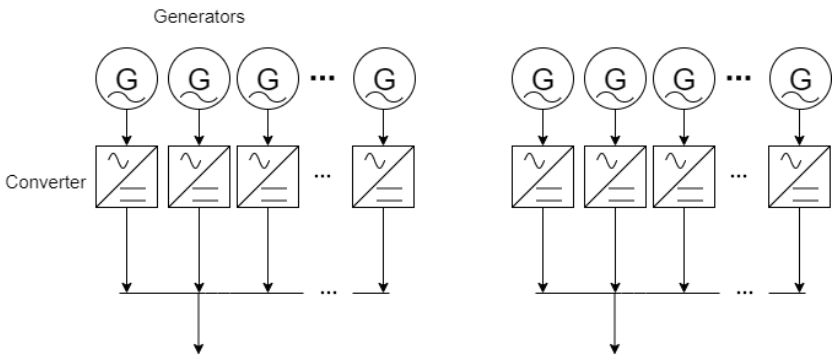

Figure 2.8. Cabling connection type 3 [25]

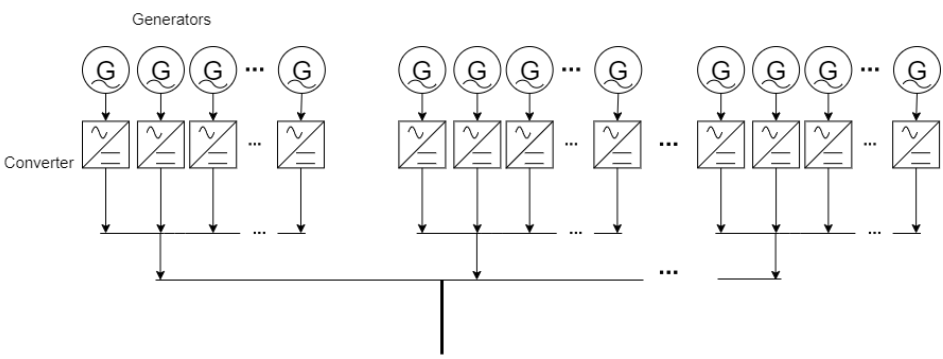

Figure 2.9. Cabling connection type 4 [25]

Based on the reliability and cable cost of the cabling connection types the following comparison can be inferred:

Table 2. *Comparison of cable connection type against availability and cable cost*

Cabling Connection	Reliability	Cable cost
Cable connection type 1	Very high	Very high
Cable connection type 2	Low	Low
Cable connection type 3	High	High
Cable connection type 4	Medium	Medium

In connection type 1, each WEC has an independent connection to shore thereby having high reliability, even if one cable fails the other WEC are not affected but due to independent cables for each WEC, the cable cost is very high. In type 2, all the WEC present are connected to a single cable which is then connected to shore. This type has low cable cost due to a smaller number of cables, but reliability is low since a single cable connects all the devices. In type 3, WEC's are grouped into clusters and each cluster is connected further by a single cable. In type 4, all clusters present in the area are connected by a single cable transmitting to shore. Due to the presence of sub clusters and individual cabling for WEC beyond that, the reliability is considered at a medium compared to other types with a medium cable cost.

3 Method

This chapter focuses on the method involved in designing and running a SWAN wave model. The various tools used as well as the numerical wave model inputs are explained.

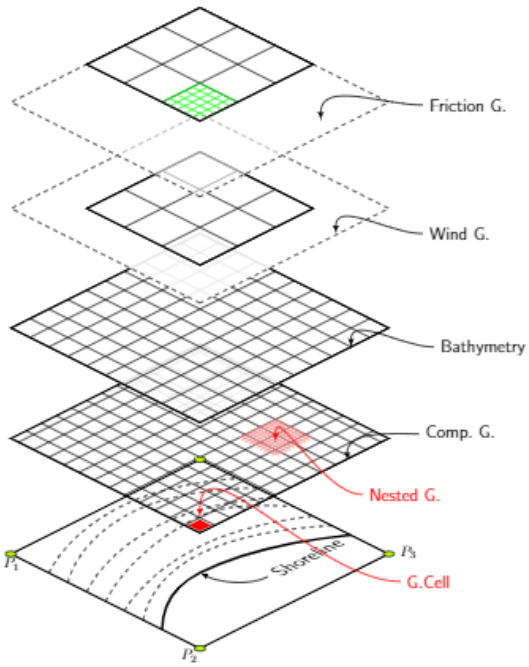

Figure 3.1. Structure of a SWAN model [26]

Figure 3.1 shows an overview of the necessary components in a SWAN model. The lowest layer consists of the land boundary in the area of interest. This includes a detailed shoreline along with any obstacles such as islands and offshore structures. This is overlaid by a computational grid. The computational grid consists of a large grid broken down into individual grid cells allowing for the numerical model to compute each grid cell based on the input parameters affecting that cell. A structured nested grid approach is used for the computational runs. A nested grid approach allows for refined grids to be imposed upon one another, so a smaller more refined grid is placed over a

larger coarse grid. This is done to improve the accuracy of a particular location within the area of interest while also decreasing computational time.

The computational grid is overlaid with bathymetry maps of the region. Bathymetry maps define the underwater depth of ocean floors and the seabed. This is overlaid by a wind grid. The wind grid can consist of uniform, time varying or space varying conditions. The SWAN model considers wind at a 10 m height and is necessary for accuracy of the results. The wind grid is overlaid by friction and other physical parameters used in SWAN. These parameters relate to the numerical modeling of the SWAN computation and factors into wave forces as well.

3.1 Inputs

3.1.1 Wind input

Wind data consists of two wind parameters: wind speed (m/s) and wind direction (°). The studied region, Hvide Sande is home to multiple wind turbines situated along its shore as well as offshore. These turbines monitor wind conditions along a 10-minute resolution at a 10 m hub height. Due to the proximity of the turbines to the area of interest and the high time resolution, the wind data from the turbines is considered for the wave computation.

A time period of 3 years is considered for the wave computation. Hence, wind input for the three years is necessary. Since the wave model is focused on a particular point (buoy location) in the area of interest over a period of time, a time varying wind input is necessary where the wind speed and direction are varied in time. The accuracy of the wind input directly relates to the accuracy of the wave model; hence it is necessary to have a high accuracy wind input.

The SWAN model uses a nautical convention of direction. Therefore, any wind data provided must be converted to a nautical convention. The wind data gathered from the turbines is plotted below for a period of three years.

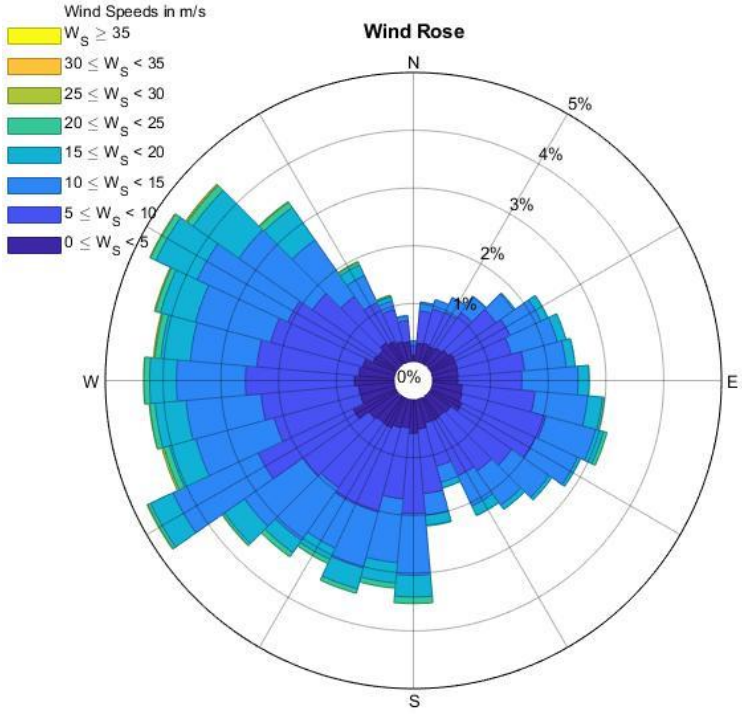

Figure 3.2. Wind rose depicting wind speed and wind direction for a three-year period (2016 - 2018)

3.1.2 Wave input

The SWAN wave model requires wave boundary conditions for proper operation of the model. The wave boundary conditions provide the wave model with the starting wave parameters necessary for computation at nearshore locations. The wave boundary conditions include significant wave height (m), wave direction (°) and wave period (s). These wave parameters are applied to the boundary of the computational grids and wave propagation is simulated. The wave data applied can be uniform, time varying and space varying. In this case due to the focus in a particular location in the area of interest, a time varying approach is used as opposed to a space and time varying approach.

The wave data used was obtained from the world wave's data source of the European Centre for Medium Range Weather Forecasts (ECMWF) for a temporal resolution of 6 hours in an area of 54° to 55° North and 7° to 8° East (off the coast of Hvide Sande).

The ECMWF maintains an open database of weather data including wave parameters such as wave height, temperature, wave period and others. The

information available through their database is gathered through a combination of wave data from buoys, satellites, and numerical modelling.

The gathered wave data is inputted to SWAN in the form of wave boundary conditions.

3.2 Grids

3.2.1 Computational grid

Prior to designing of the computational grid, a land boundary of the area of interest must be created.

Open source tools such as google earth can be used to map out the coastline as well as any obstacles in the region. This helps create a discernable layout and allows for design of the computational grid.

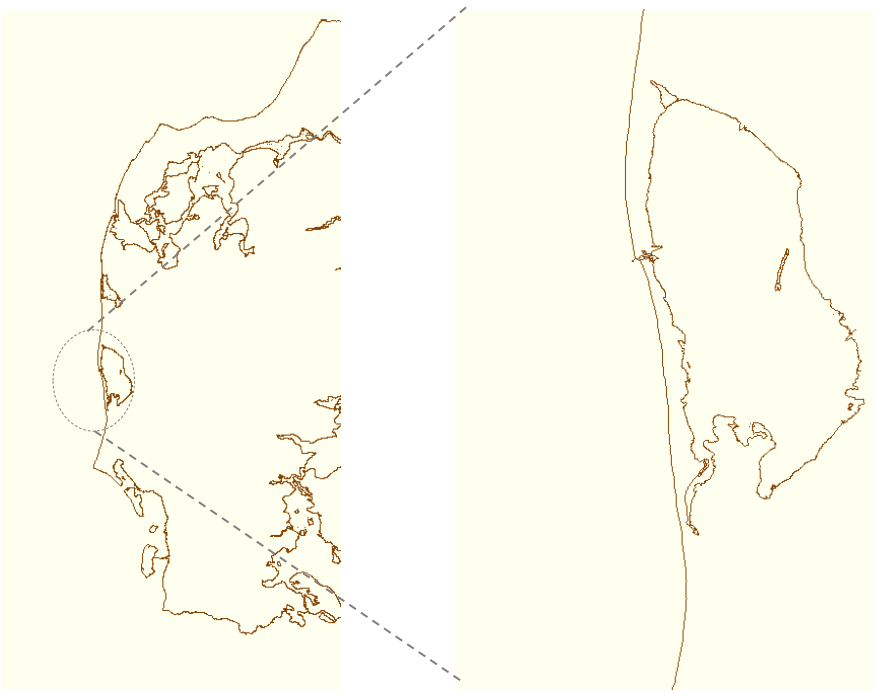

Figure 3.3. Land boundary file for the region of Hvide Sande
(left) Land boundary of Denmark
(right) Land boundary depicting the coastline of Hvide Sande

From the land boundary of Hvide Sande we can design the computational grid boundaries. The grid boundaries can be superimposed on the land boundary

file and any points of interest in the region can be centered in the grid boundary.

The grid boundary can be designed and created using AutoCAD which allows for precise demarcations as well as to consider distance from shore.

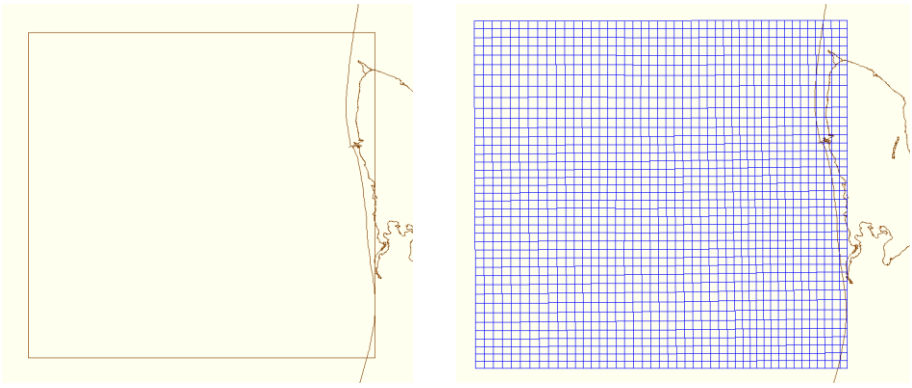

Figure 3.4. (left) Grid boundary covering coastline of Hvide Sande
(right) Grid cells created using grid boundary

Following the grid boundary, the grid cells can be generated within the grid boundary. This is done by using the RGFGRID tool in the Delft3D platform. The tool uses a boundary fitted grid generation method to create a structured grid within the created boundary. The refinement factor can be varied to increase or decrease the refinement of the grid. The grid can also be locally refined allowing for only regions of interest within the grid to be highly refined. The creation of the grid cells from the grid boundary is shown in Figure 3.4.

The planned SWAN computation uses a nested approach which requires the creation of multiple refined grids, nested in each other. In a nested approach, the results of the SWAN computation are provided as input boundaries to the smaller grid, this allows for a higher accuracy output while lowering simulation time. Keeping the buoy location centered, multiple grids with increasing refinement factors are created and nested.

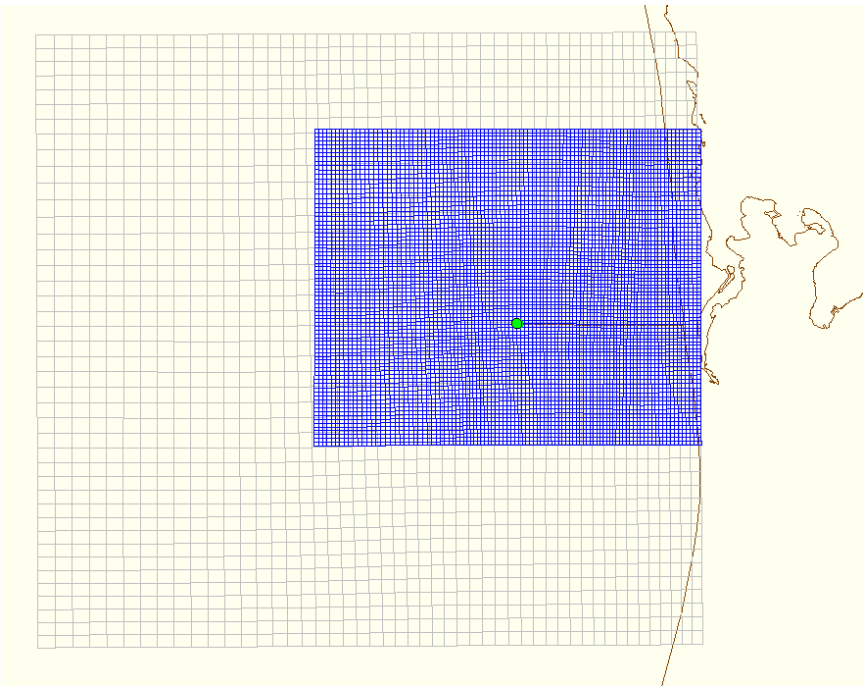

Figure 3.5. Nested grid approach with a highly refined grid nested in a larger coarse grid, buoy location marked and centered

The designed grid consists of two grids. The larger grid is less refined and includes the entire region of interest. This is done to include any bathymetry and wind, wave input that affects the output at the point location. A square shape grid is chosen due to the simplicity of the design. The smaller more refined grid is overlaid on top of the coarse grid. The smaller grid consists of smaller grid cells due to a higher refinement. This helps in better integrating input data as well as coinciding bathymetry thereby increasing accuracy. Further increasing the refinement grid leads to a negligible increase in accuracy but at a much higher simulation time.

3.2.2 Bathymetry grid

The generation of bathymetry maps of the region are done by using Delft dashboard, which is a MATLAB based graphical user interface (GUI) which consists of coupled toolboxes that allow for model generation.

Open source world bathymetry maps can be accessed through the dashboard and the bathymetry dataset for the region of interest can be generated.

Figure 3.6 below shows the bathymetry map in the region of Hvide Sande. The darker red colors relate to deeper waters and it can be observed that the depth reduces as it approaches the shore.

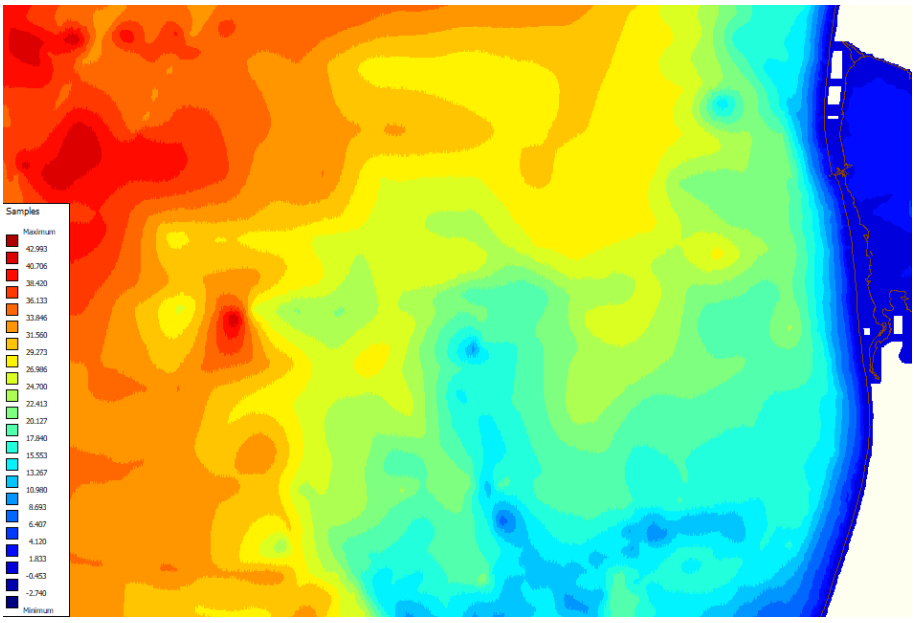

Figure 3.6. Generated bathymetry map of the region of Hvide Sande

On generation of bathymetry maps, bathymetry needs to be imposed onto the computational grid. This is done to embed the grid cells with the coinciding bathymetry data. Delft3D is used to perform data interpolation to the computational grid.

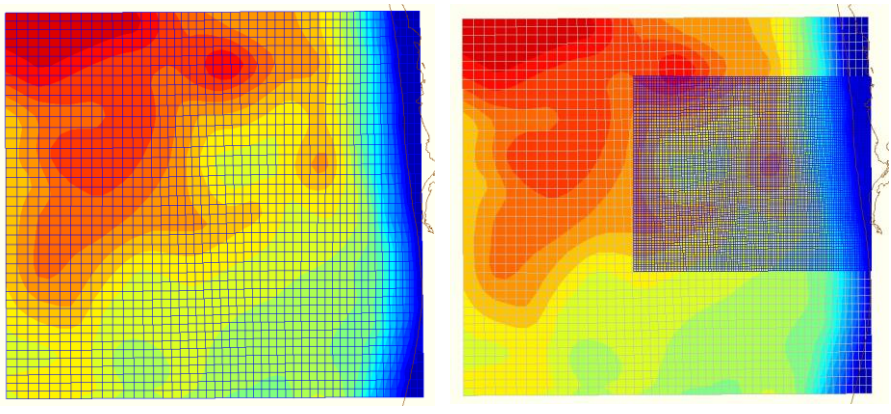

Figure 3.7. Integration of bathymetry maps into the computational grid
(left) Integration of bathymetry into the coarse grid
(right) nested grids with integrated bathymetry

3.3 SWAN parameters

Once the necessary inputs have been integrated into the SWAN model, the model must be calibrated. The different physical and numerical parameters affect the output of the computational model.

The parameters can involve the use of a parametric 1D spectrum with directional distribution or a discrete 1D spectrum with directional distribution. For the parametric approach, a form such as Jonswap or Pierson-Moskowitz spectrum is used. Another approach utilizes a discrete 2D spectrum requiring the use of a previous SWAN run or other wave models. Hence, the region and the output requirements impact the parameters used.

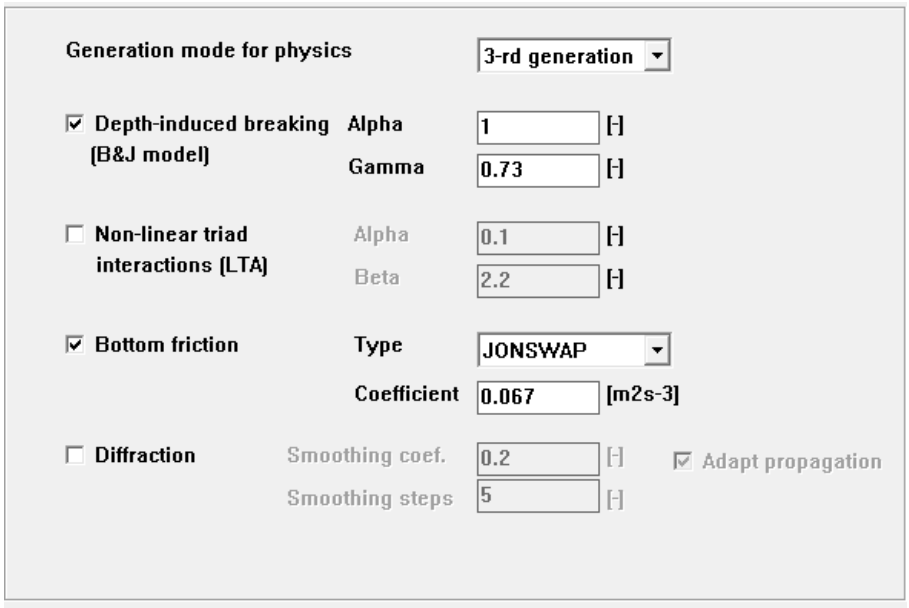

Figure 3.8. Physical parameters being utilized by SWAN

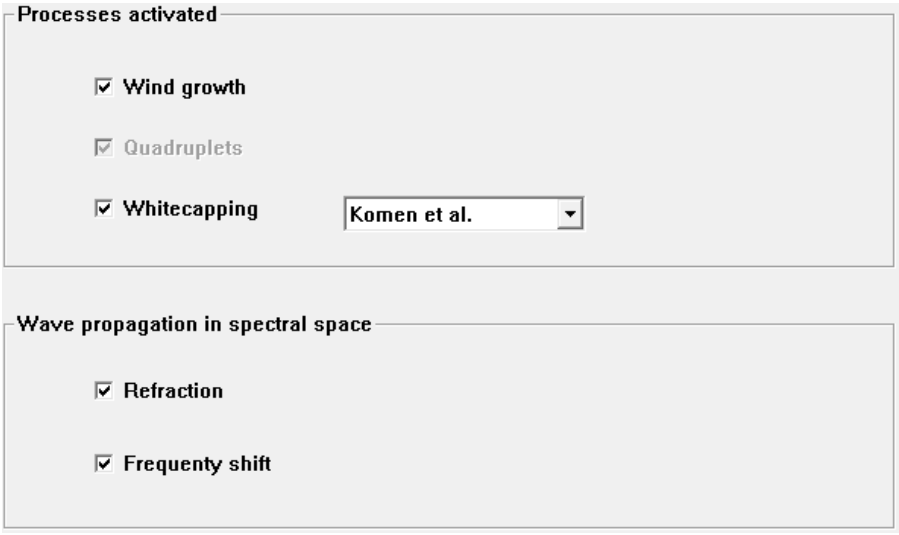

Figure 3.9. Process parameters being utilized by SWAN

4 Results & Discussion

The results are focused on two wave parameters: wave height and wave period. The energy flux of ocean waves is given by:

$$J = \frac{\rho g^2}{64\pi} T_E H_s^2 \tag{4.1}$$

where J is the energy flux (W/m), ρ is the density of sea water at 1025 kg/m^3, g is the acceleration due to gravity and T_E is the energy period (s) with the wave height being denoted by H_s.

The energy flux given by watt per meter of crest length resembles the wave energy in the area. The wave period and wave height are directly proportional to the energy flux with the wave height having a larger significance on the energy flux.

The results will compare the calculated wave parameters of the numerical model against that of the measured buoy data.

Initially, the numerical wave model is used to calculate the wave height in the area of interest. The calculated wave height is then compared with the measured buoy wave height. The comparative analysis is done to understand the effect of the physical parameters and different approaches utilized by SWAN. This then can be used to improve the accuracy of the results for the area of interest. This is followed by a comparative analysis on wave period as well as calculated energy flux at the location. The results conclude with a scatter diagram that provides an estimate of the power generation available at the location.

4.1 SWAN computations

4.1.1 Test run 1

This test run was done for a period of 24 hours for 01 January 2018. A spatially constant but time varying wind condition is applied along with a constant boundary condition. The constant and uniform wave boundary conditions

used include wave height of 8.66 m and a wave period of 6.93 s. A wave direction of 270° was used to simulate wave propagation from west to east.

This run focused on the different grid directional spectral resolution available and the effect of physical parameters whitecapping, LTA and diffraction on the results. The following results were observed:

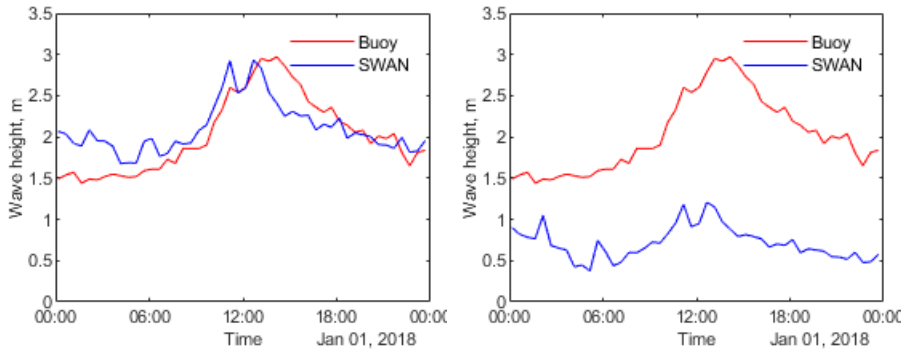

Figure 4.1. SWAN run with different directional space
(left) circular directional space in spectral resolution
(right) sector directional space from 0° to 180° in spectral resolution

Figure 4.1 above shows the changes in directional space of spectral resolution. It is clear that, a circular directional space is preferred in this case as compared to a sector based directional space with the start direction at 0° and end direction at 180°. Further test runs on this showed the results to be consistent for all test runs for a circular resolution while results for a sector resolution varied based on the start and end direction. Hence, a circular resolution space will be considered for future runs.

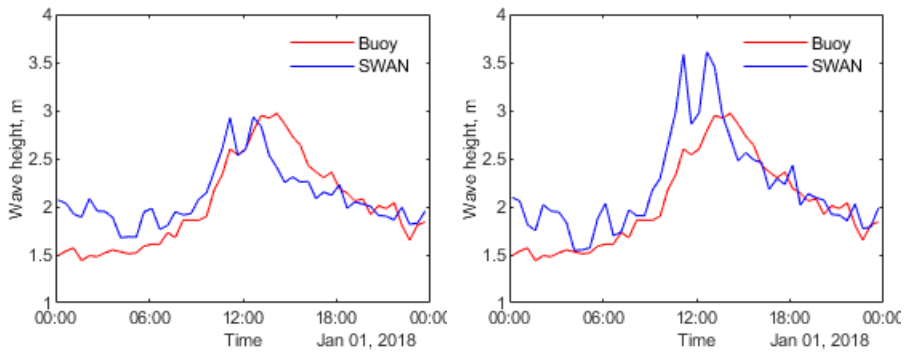

Figure 4.2. SWAN run with whitecapping enabled or disabled
(left) whitecapping enabled during SWAN run
(right) whitecapping disabled during SWAN run

Figure 4.2 above shows the change in the calculated data with whitecapping turned on and with whitecapping turned off. It is clear that with whitecapping disabled, the calculated SWAN data is much higher in comparison to the buoy data. Other test runs on this confirmed that disabling whitecapping significantly increases the wave height beyond the measured value in all cases. Hence, whitecapping is enabled for future simulations.

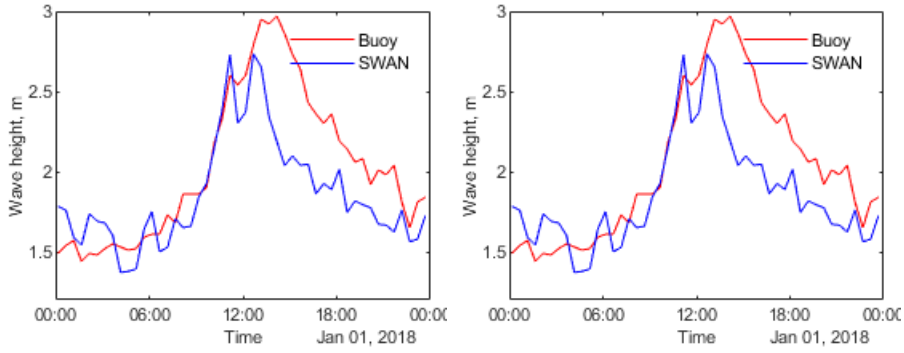

Figure 4.3. SWAN run with linear triad interaction and diffraction parameters
(left) SWAN run with default parameters enabled
(right) LTA and diffraction parameters disabled

In this case the effect of linear triad interaction (LTA) and diffraction are studied. There is no discernable difference in the results when LTA, diffraction is enabled and when they are disabled. Based on this, LTA and diffraction are disabled for future runs.

4.1.2 Test run 2

This test run was done for another period of 24 hours for 01 June 2017. A spatially constant but time varying wind condition is applied along with constant boundary condition. The constant and uniform wave boundary conditions used include a wave height of 1.8 m and a wave period of 6.93 s. This wave spectra was chosen as the most optimal for this time period after multiple tests were conducted with default SWAN parameters and varying wave spectra. A wave direction of 275° was used to simulate wave propagation from west to east.

Based on the results of test run 1, a circular spectral resolution is used with whitecapping enabled. LTA and diffraction parameters are disabled. This run focused on the bottom friction and depth breaking parameters used in SWAN. The test was conducted, and the following results were observed.

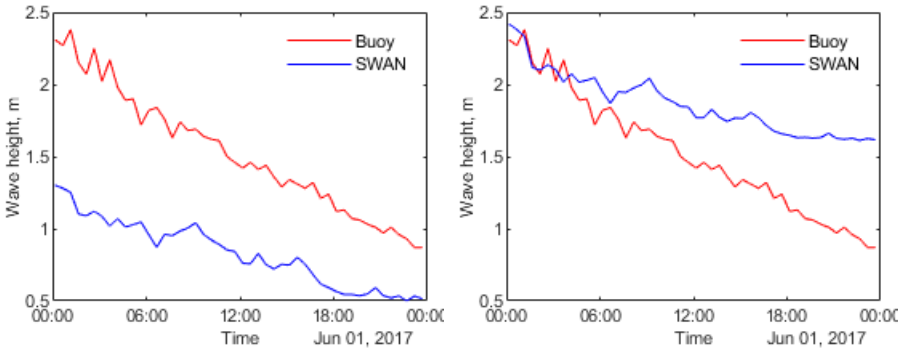

Figure 4.4. SWAN run with varying bottom friction
(left) SWAN run with JONSWAP bottom friction coefficient of 9 $m^2 s^{-3}$
(right) SWAN run with JONSWAP bottom friction coefficient of 0.067 $m^2 s^{-3}$

Figure 4.4 above shows the changes in the wave height based on different bottom friction coefficients used. It was found that a bottom friction JONSWAP approximation with a coefficient of 0.067 $m^2 s^{-3}$ provides the best approximation to the measured value.

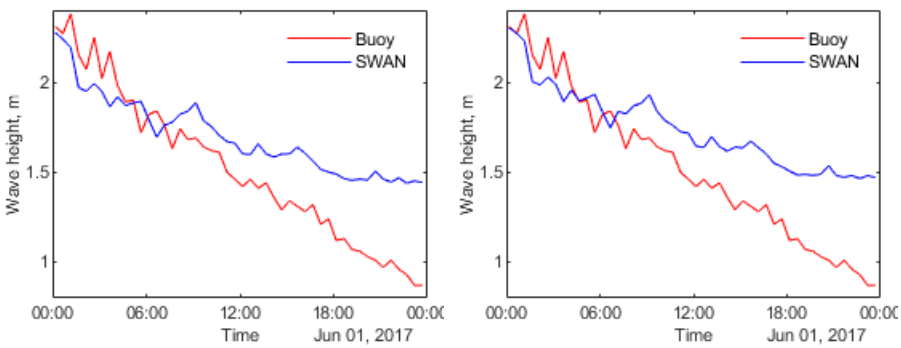

Figure 4.5. SWAN run with varying coefficient of depth-induced breaking
(left) SWAN run with depth-induced breaking value at 9
(right) SWAN run with-depth induced breaking at 1 (default value)

The change in depth induced breaking coefficient has a negligible impact on the wave height. The default value of depth breaking is used in future simulations.

Based on test run 2, we can conclude that a JONSWAP bottom friction coefficient of 0.067 and a depth induced breaking coefficient of 1 are the preferred parameters.

Test runs 1 & 2 were focused on the effects of physical and numerical parameters on the SWAN computational results. The results of the test runs along

with multiple other runs conclude that the optimal parameters for the region include:

- Circular spectral direction
- Whitecapping enabled
- LTA and diffraction disabled
- JONSWAP breaking coefficient set at 0.067 $m^2 s^{-3}$
- Depth induced breaking at default value of 1

The test runs were performed at different time periods to account for varying input conditions and its effect on the results. It was found that the parameters mentioned above remained the optimal parameters for the region despite changes in time period and input conditions.

4.1.3 Test run 3

This test run focuses on the significance of wave boundary conditions and its effect on SWAN computational results. The test run is carried out for a time period of 24 hours for 01 June 2017. The physical and numerical parameters defined from the previous runs are used here. Hence, any changes in the following results are dependent on changes in wave boundary conditions.

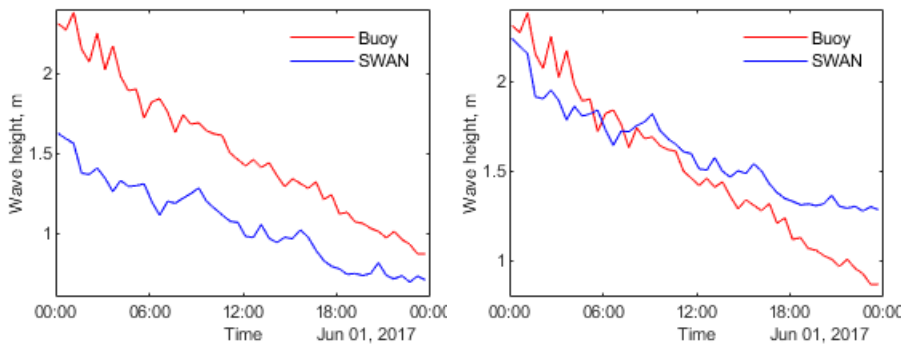

Figure 4.6. SWAN run with different wave boundary conditions
(left) SWAN run with boundary wave height of 1.8 m and wave direction of 200°
(right) SWAN run with boundary wave height of 1.7 m and wave direction of 300°

Figure 4.6 above shows a significant difference in the SWAN computational results based on different wave boundary conditions. Further simulations were done based on this with different time periods and it was found that, accuracy of the results are highest for its corresponding wave boundary. Since, the time period varies during a computational run, a time varying wave boundary condition needs to be implemented. This is done by using wave data gathered from the European Centre for Medium Range Weather Forecasts (ECMWF).

Time varying wave boundary condition is then implemented in the following run along with the previously chosen physical and numerical parameters. The run was carried out for a period of 4 months from 01 February 2017 to 31 May 2017.

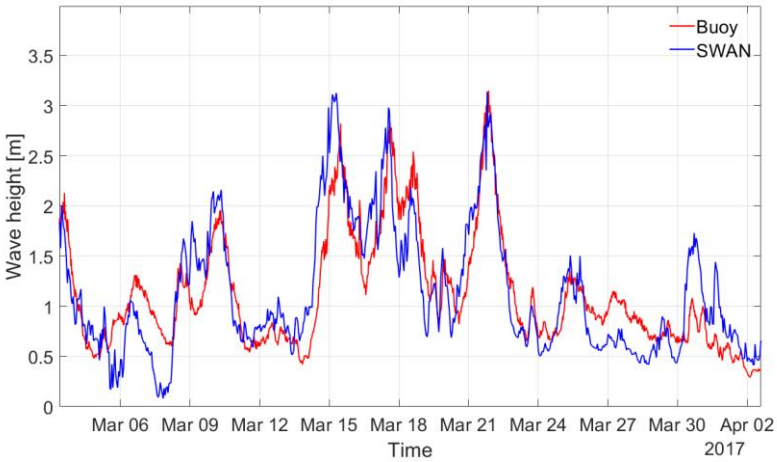

Figure 4.7. SWAN computation output using time varying wave boundary conditions

4.1.4 Accuracy of the numerical prediction

To better discern the difference in results, the accuracy of the numerical predictions for different approaches is found. This is done by using two values [27]. The correlation coefficient calculated by:

$$R = \frac{\sum_{i=1}^{N}(x_i - \bar{x})(y_i - \overline{y})}{\sqrt{\sum_{i=1}^{N}(x_i - \bar{x})^2 \sum_{i=1}^{N}(y_i - \bar{y})^2}} \tag{4.2}$$

Where x_i is the calculated data and y_i is the measured buoy data. $\bar{x}$ & $\bar{y}$ relate to the mean value of the data.

The correlation coefficient ranges from -1 to 1. A value closer to 1 resembles a higher accuracy with the compared data while a value closer to -1 resembles a low accuracy.

The other value used is the relative square root error (RRE) [27]. This is given by:

(4.3)

$$RRE = \sqrt{\frac{\sum_{i=1}^{N}(y_i - x_i)^2}{\sum_{i=1}^{N}(y_i - \bar{y})^2}}$$

In case of RRE, a value closer to 0 indicates less error between the measured and calculated values.

The accuracy of the numerical predictions is carried out at the end of the each of the previous test runs. The following results were observed:

Table 3. *Computational accuracy of previous test runs*

	Corelation coefficient	Relative square root error
Test run 1	0.5859	0.9761
Test run 2	0.8327	0.8753
Test run 3	0.9108	0.0188

Table 3 shows that the accuracy of the results improving upon each run with test run 3 having the highest accuracy. It is observed that the largest accuracy increase in both correlation coefficient and RRE values is through test run 3 with the implementation of a time varying wave boundary.

To further increase the accuracy of the computational results, the wave boundary orientation and boundary reflection factors are considered. Further computational simulations are carried out with different boundary orientation and multiple boundary parameters.

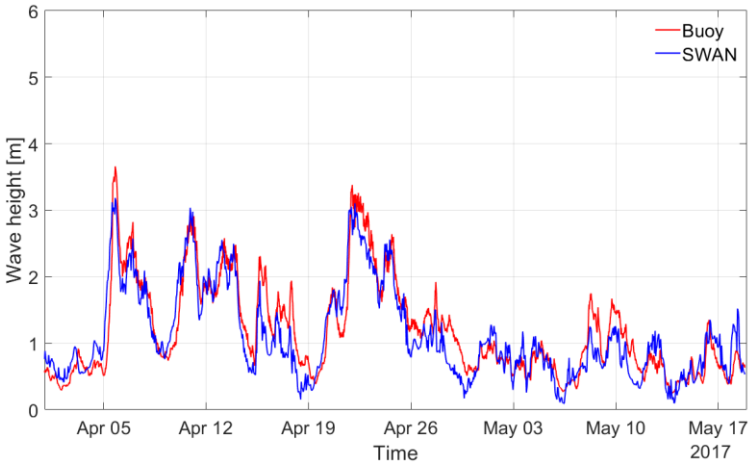

Figure 4.8. SWAN computation of test run 4 using a single boundary approach

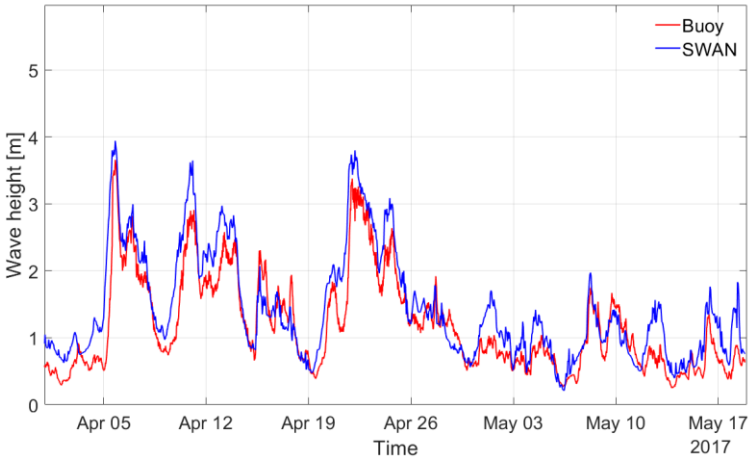

Figure 4.9. SWAN computation of test run 5 using multiple boundary approach

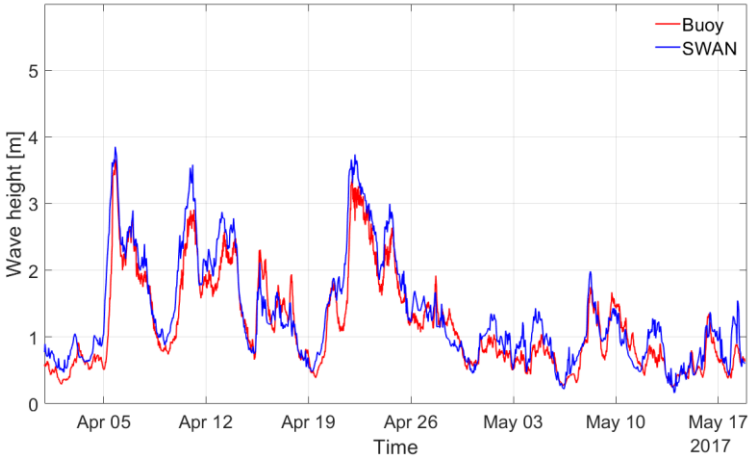

Figure 4.10. SWAN computation of test run 6 using multiple boundary approach with a westerly orientation

Due to the smaller change in accuracy between these results, the accuracy of the results is discerned using the correlation coefficient and RRE values.

Table 4. *Computational accuracy of runs with different boundary approaches*

	Corelation coefficient	Relative square root error
Test run 4	0.9108	0.0188
Test run 5	0.9204	0.0176
Test run 6	0.9387	0.0101

Table 4 shows that trial run 6 has the highest accuracy utilizing multiple boundaries with a westerly orientation. These results conclude that the test runs with the most optimal parameters for the SWAN computation for this region is as follows:

- Time varying wave boundary conditions
- Multiple boundary inputs
- Circular spectral direction
- Whitecapping enabled
- LTA and diffraction disabled
- JONSWAP breaking coefficient set at 0.067 $m^2 s^{-3}$
- Depth induced breaking at default value of 1

4.1.5 SWAN computation for a three-year period

Following the results of the trial runs, a longer computational model is run for a period of 3 years from 01 Jan 2016 to 31 Dec 2018. The previously listed parameters are used for this simulation. The time varying boundary condition is inputted for a 6-hour temporal resolution. Some of the results of the simulation are shown below:

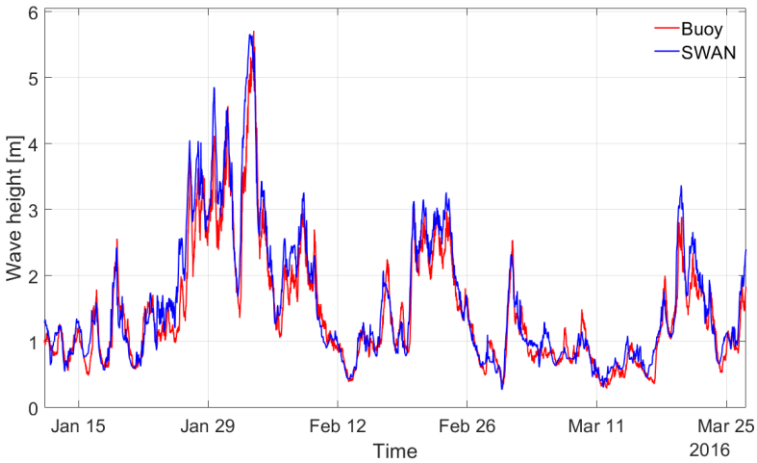

Figure 4.11. SWAN computational result vs buoy measured data during the period of 2016

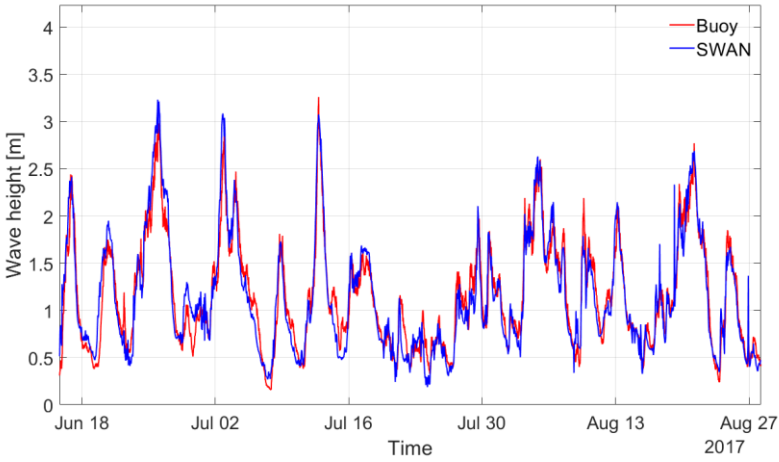

Figure 4.12. SWAN computational result vs buoy measured data during the period of 2017

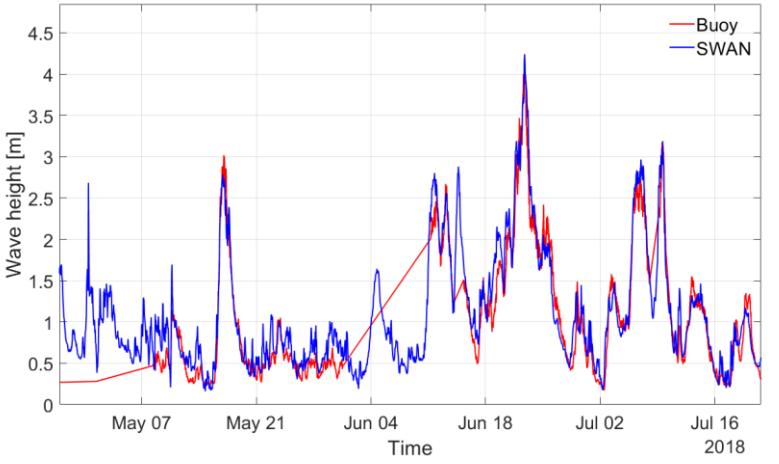

Figure 4.13. SWAN computational result of wave height vs buoy measured data during the period of 2018

Part of the measured buoy data is missing, hence the inaccuracy of the buoy data in Figure 4.13

The results of the SWAN computation show that the accuracy of the computed wave model is very high and is comparable to that of measured data obtained from a wave buoy. I can conclude that assessment of wave height using numerical wave modeling is comparable to that of a wave buoy in terms of accuracy but is far cheaper and less time dependent than that of wave buoys. I can further conclude that numerical wave modeling is less prone to wave height inaccuracies caused by the movement of ships and other factors, and as seen from Figure 4.13 above, wave buoys are also prone to data loss.

4.1.5.1 Energy period and energy flux

The energy period can also be calculated through the numerical wave model. The SWAN model computes both wave height as well as energy period in the same computation. Since, the accuracy of wave height was optimized for the region, the resultant energy period for the same are seen in Figure 4.14.

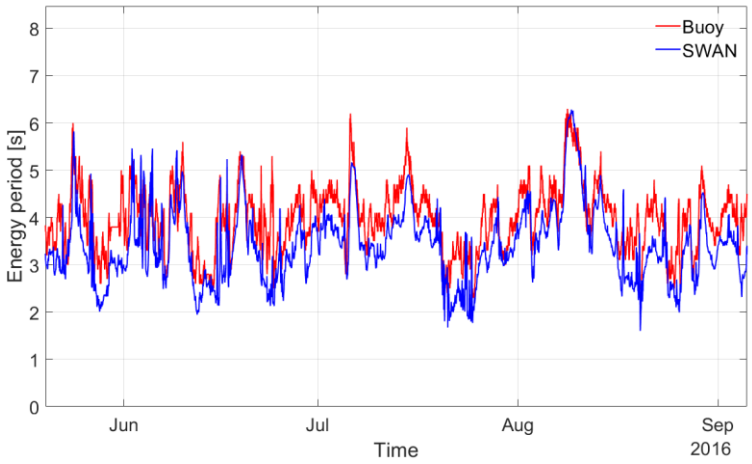

Figure 4.14. SWAN computational result of energy period vs measured buoy data during the period of 2016

Based on the calculated sig. wave height and energy period. Energy flux can be calculated using eq. 4.1. The resultant calculated energy flux is compared against that of buoy data.

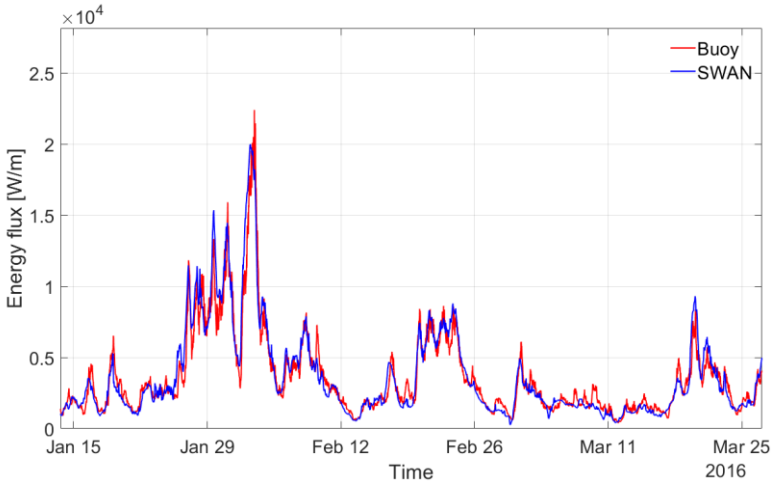

Figure 4.15. Calculated energy flux of the SWAN computational model vs buoy data

4.2 Scatter diagram

Scatter diagrams for the area of interest are plotted to understand the occurrence of different significant wave heights and energy periods. The energy period and significant wave height has both been divided into intervals of 0.5 s and 0.5 m respectively. The colors indicate the occurrence of the combination of wave height and energy period marked by the color bar. The contour lines across the scatter diagram is the energy flux which is calculate using eq. 4.1.

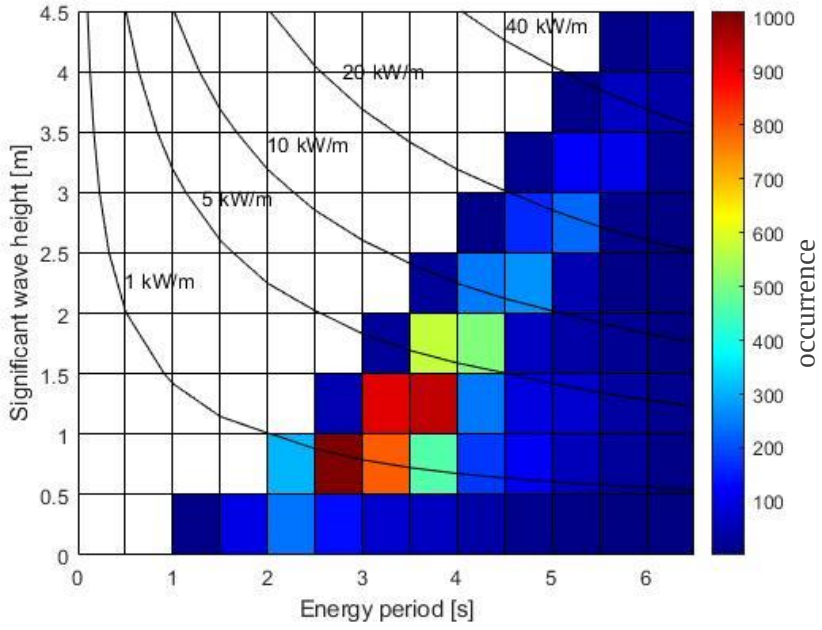

Figure 4.16. Scatter diagram of significant wave height and energy period for the year 2016

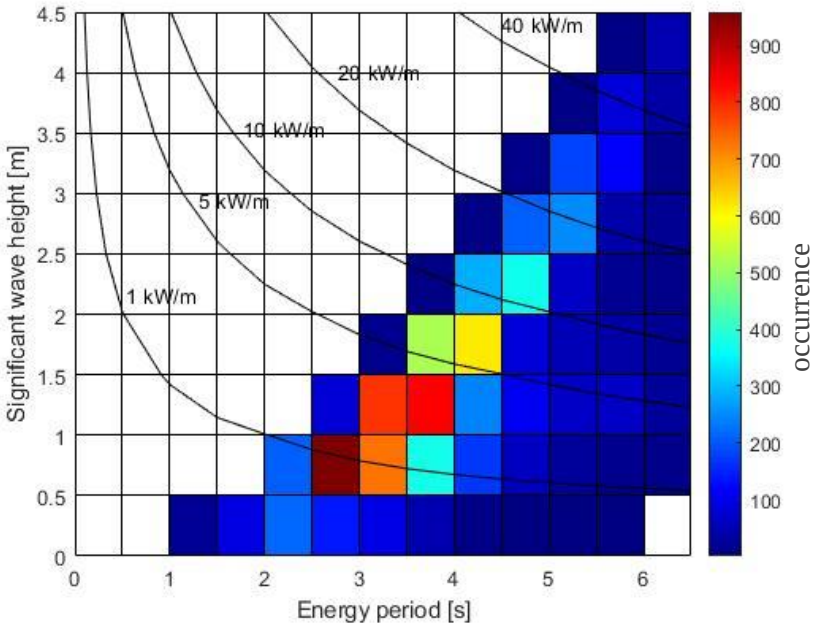

Figure 4.17. Scatter diagram of significant wave height and energy period for the year 2017

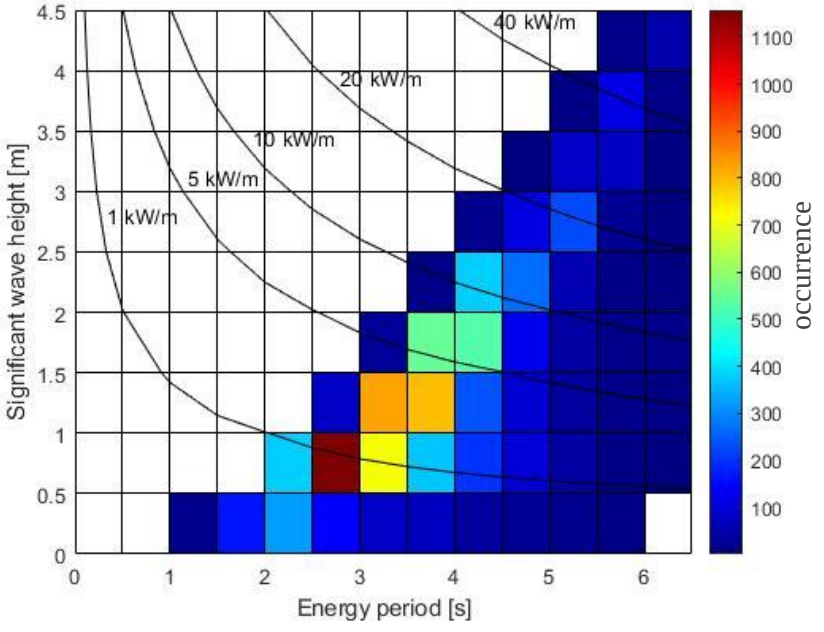

Figure 4.18. Scatter diagram of significant wave height and energy period for the year 2018

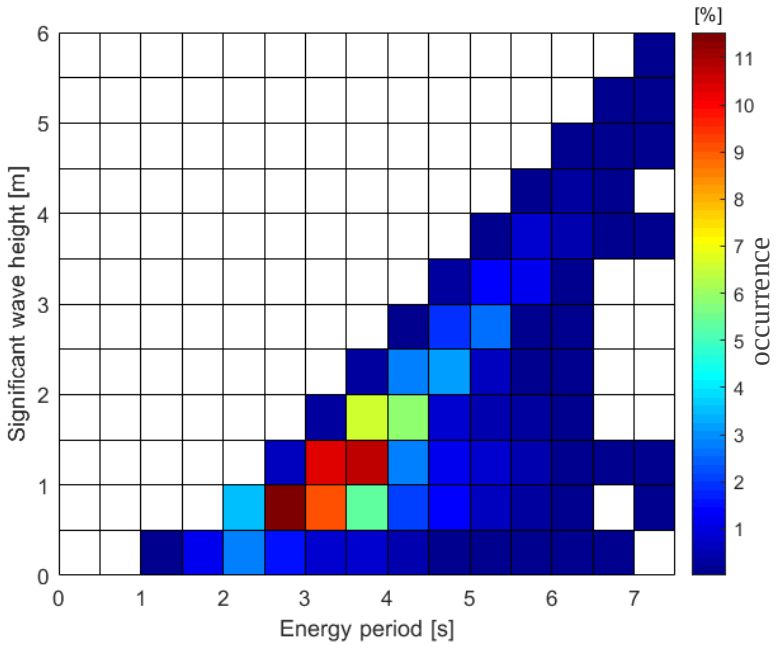

Figure 4.19. Scatter diagram of significant wave height and energy period over the time period of three years with the stated frequency of occurrence in %

Figures 4.16, 4.17, 4.18 show the scatter diagrams for the years 2016, 2017 and 2018 respectively. The scatter diagram shows the frequency of occurrence of a particular combination of wave height and energy period. From this I can estimate the energy flux available within the region for the time period by considering the most frequently occurring wave states in the region.

Figure 4.19 shows the scatter diagram for the combined period of 2016, 2017 and 2018 with the frequency of occurrence depicted in percentage. It was found that the most frequent sea states due to calculated results are Hs 0.5 to 1.5 m and Te 2.5 to 4 s with the rate of concurrency of 12 %. Second most frequent sea state is more energetic with Hs 1.5 to 2 m and Te 3.5 to 4 s with the rate of 7 % for the three-year calculation time period. This corresponds to an energy flux of 1 to 5 kW/m.

The amount of generated power from the region would depend on the type of point absorber design and dimensions. In the study [28], it was found that for a passive rectification, a 25% absorption of wave power could be achieved.

5 Conclusion

Wave resource assessment using computation model SWAN has been performed for the area of study located in Hvide Sande, Denmark. Comparative analysis using correlation coefficient and calculated relative square root error has been done to detect the best result with the highest accuracy. Detailed description of the methodology was presented along with used computational parameters of the numeric wave model. Wave climate scatter diagram was calculated for the time period of three years (2016-2018) and the most frequent sea states were found. The corresponding energy flux to the most frequent sea states was found to be in the range of 1-5 kW/m and the highest energy flux for the area is about 40 kW/m.

6 References

[1] "Energy - Our World in Data." https://ourworldindata.org/energy (accessed Sep. 20, 2020).

[2] "Wave energy - Ocean Energy Europe." https://www.oceanenergy-europe.eu/ocean-energy/wave-energy/ (accessed Sep. 20, 2020).

[3] B. Robertson, "Wave energy assessments: Quantifying the resource and understanding the uncertainty," in *Marine Renewable Energy: Resource Characterization and Physical Effects*, Springer International Publishing, 2017, pp. 1–36.

[4] E. B. L. Mackay, "Resource assessment for wave energy," in *Comprehensive Renewable Energy*, vol. 8, Elsevier Ltd, 2012, pp. 11–77.

[5] R. Waters, J. Engström, J. Isberg, and M. Leijon, "Wave climate off the Swedish west coast," *Renewable Energy*, vol. 34, no. 6, pp. 1600–1606, Jun. 2009, doi: 10.1016/j.renene.2008.11.016.

[6] "Wave Buoys: Pitfalls, Price Tags and Piracy on the High Seas." https://www.miros-group.com/blog/wave-buoys-pitfalls-price-tags-and-piracy-on-the-high-seas/ (accessed Sep. 22, 2020).

[7] T. J. Thomas and G. S. Dwarakish, "Numerical Wave Modelling – A Review," *Aquatic Procedia*, vol. 4, pp. 443–448, Jan. 2015, doi: 10.1016/j.aqpro.2015.02.059.

[8] "Assessment of Wave Energy Resource : EMEC: European Marine Energy Centre." http://www.emec.org.uk/assessment-of-wave-energy-resource/ (accessed Sep. 22, 2020).

[9] "SWAN." https://www.tudelft.nl/en/ceg/about-faculty/departments/hydraulic-engineering/sections/environmental-fluid-mechanics/research/swan/ (accessed Sep. 22, 2020).

[10] F. Francisco, J. Leijon, C. Boström, J. Engström, and J. Sundberg, "Wave Power as Solution for Off-Grid Water Desalination Systems: Resource Characterization for Kilifi-Kenya," *Energies*, vol. 11, no. 4, p. 1004, Apr. 2018, doi: 10.3390/en11041004.

[11] "Wave power concept - Section of Technology - Uppsala University, Sweden." https://www.teknik.uu.se/electricity/research-areas/wave-power/wave-power-concept/ (accessed Sep. 25, 2020).

[12] M. Rahm, "Ocean Wave Energy: Underwater Substation System for Wave Energy Converters." Accessed: Sep. 25, 2020. [Online].

[13] "Datawell Directional Waverider Manual," 2005.

[14] "Spectral action balance equation." http://swanmodel.sourceforge.net/online_doc/swantech/node12.html (accessed Sep. 24, 2020).

[15] "Historical background." http://swanmodel.sourceforge.net/online_doc/swantech/node2.html (accessed Sep. 22, 2020).
[16] "General concepts." http://swanmodel.sourceforge.net/online_doc/swantech/node14.html (accessed Oct. 15, 2020).
[17] H. L. Tolman, "Effects of numerics on the physics in a third-generation wind-wave model," *Journal of Physical Oceanography*, vol. 22, no. 10, pp. 1095–1111, Oct. 1992, doi: 10.1175/1520-0485(1992)022<1095:EONOTP>2.0.CO;2.
[18] K. Hasselmann, "On the spectral dissipation of ocean waves due to white capping," *Boundary-Layer Meteorology*, vol. 6, no. 1–2, pp. 107–127, Mar. 1974, doi: 10.1007/BF00232479.
[19] Hasselmann and al, "Measurements of wind-wave growth and swell decay during the Joint North Sea Wave Project (JONSWAP)," Deutches Hydrographisches Institut, 1973. Accessed: Sep. 23, 2020. [Online]. Available: https://repository.tudelft.nl/islandora/object/uuid%3Af204e188-13b9-49d8-a6dc-4fb7c20562fc.
[20] O. S. Madsen, Y.-K. Poon, and H. C. Graber, "Spectral Wave Attenuation by Bottom Friction: Theory," in *Coastal Engineering 1988*, Nov. 1989, pp. 492–504, doi: 10.1061/9780872626874.035.
[21] J. A. Battjes and J. P. F. M. Janssen, "Energy Loss and Set-Up Due to Breaking of Random Waves," in *Coastal Engineering 1978*, Aug. 1978, pp. 569–587, doi: 10.1061/9780872621909.034.
[22] O. Farrok, K. Ahmed, A. D. Tahlil, M. M. Farah, M. R. Kiran, and Md. R. Islam, "Electrical Power Generation from the Oceanic Wave for Sustainable Advancement in Renewable Energy Technologies," *Sustainability*, vol. 12, no. 6, p. 2178, Mar. 2020, doi: 10.3390/su12062178.
[23] Hmarcollo, https://upload.wikimedia.org/wikipdia/comons/thumb/5/59/WECs-2020.png/1920px-WECs-2020.png (accessed Sep. 25, 2020).
[24] M. Penalba and J. Ringwood, "A Review of Wave-to-Wire Models for Wave Energy Converters," *Energies*, vol. 9, no. 7, p. 506, Jun. 2016, doi: 10.3390/en9070506.
[25] K. Thorburn, H. Bernhoff, and M. Leijon, "Wave energy transmission system concepts for linear generator arrays," *Ocean Engineering*, vol. 31, no. 11–12, pp. 1339–1349, Aug. 2004, doi: 10.1016/j.oceaneng.2004.03.003.
[26] Marco Miani, "SWAN wave model | TikZ example." https://texample.net/tikz/examples/swan-wave-model/ (accessed Sep. 27, 2020).
[27] W. Sheng, R. Alcorn, and A. Lewis, "A new method for radiation forces for floating platforms in waves," *Ocean Engineering*, vol. 105, pp. 43–53, Jul. 2015, doi: 10.1016/j.oceaneng.2015.06.023.

[28] R. Ekström and M. Leijon, “Control of offshore marine substation for grid-connection of a wave power farm,” *International Journal of Marine Energy*, vol. 5, pp. 24–37, Apr. 2014, doi: 10.1016/j.ijome.2014.04.001.